


Article

Effect of Ni-MOF Derivatives on the Electrochemical Corrosion Behavior of Sn-0.7Cu Solders

Guoge Lu ¹, Bo Lin ¹, Zhan Gao ¹, Yingxin Li ¹ and Fuxiang Wei ^{1,2,*} 

¹ School of Materials and Physics, China University of Mining & Technology, Xuzhou 221116, China; 17826263672@163.com (G.L.); linbol1996@163.com (B.L.); gaozhancumt@163.com (Z.G.); liyingxin199803@163.com (Y.L.)

² Jiangsu Province Engineering Laboratory of High Efficient Energy Storage Technology and Equipments, China University of Mining and Technology, Xuzhou 221116, China

* Correspondence: weifuxiang2001@163.com

Abstract: The corrosion resistance of solder joints is a critical factor affecting the service life of electronic products during long-term operation. In this study, the corrosion behavior of Sn-0.7Cu- x Ni@C ($x = 0, 0.04, 0.08$, and 0.12 wt.%) composite solders was investigated using a Tafel polarization curve in 3.5 wt.% NaCl solution, and the result demonstrated that it was the Ni@C that enhanced the corrosion resistance of the composite solder. The corrosion rate of the composite solders decreased with increasing Ni@C content and reached the lowest value of 0.205 mm/y when the content of Ni@C reached 0.08 wt.%. Ni@C changed the morphologies of corrosion products $\text{Sn}_3\text{O}(\text{OH})_2\text{Cl}_2$ from thick flakes to dense fine needles and flakes, which made it more difficult for Cl^- to break down corrosion products. Thus, the corrosion resistance of composite solder was improved. The carbon skeleton in Ni@C served as an inert physical barrier to inhibit further corrosion. Furthermore, the potential difference between IMC and β -Sn decreased with the addition of Ni@C, which reduced the corrosion rate of the electric couple and enhanced the corrosion resistance of the composite solder.

Keywords: Sn-0.7Cu; Ni@C addition; microstructure; corrosion behavior



Citation: Lu, G.; Lin, B.; Gao, Z.; Li, Y.; Wei, F. Effect of Ni-MOF Derivatives on the Electrochemical Corrosion Behavior of Sn-0.7Cu Solders. *Metals* **2022**, *12*, 1172. <https://doi.org/10.3390/met12071172>

Academic Editor: Wislei Riuper Osório

Received: 14 June 2022

Accepted: 8 July 2022

Published: 10 July 2022

Publisher's Note: MDPI stays neutral with regard to jurisdictional claims in published maps and institutional affiliations.



Copyright: © 2022 by the authors. Licensee MDPI, Basel, Switzerland. This article is an open access article distributed under the terms and conditions of the Creative Commons Attribution (CC BY) license (<https://creativecommons.org/licenses/by/4.0/>).

1. Introduction

Sn-Pb solder is widely used in electronic packaging due to its low cost, low melting temperature and excellent wettability [1,2]. However, Pb has gradually received widespread concern for its toxicity, and thus the European Union issued directives such as Restriction of Hazardous Substances (RoHS) and Waste Electrical and Electronic Equipment (WEEE) to ban the use of Pb in electronic products [3]. Therefore, research on lead-free solder has become a popular trend in the electronics industry. Lead-free solder mainly includes SnCu [4,5], SnAgCu [6,7], SnAg [8], SnZn [9], etc., systems, among which SnCu solder is expected to replace SnPb solder due to its low cost, high strength, and low resistivity [10]. However, electronic products such as communication equipment and control equipment of ships are exposed to humid corrosive media, which increases the need for the corrosion resistance of SnCu solder [11].

It has been reported that carbon-based materials (CNTs, GNS) and metal particles (Ni, Co, Ag, Bi, In) can improve the corrosion resistance of lead-free solder [12–14]. Han et al. [15] added 0.01 wt.%, 0.03 wt.%, and 0.07 wt.% of Ni-CNTs, respectively, to Sn-Ag-Cu solder. It was found that the microstructure of the composite solder is refined and the corrosion rate reduced with the addition of Ni-CNTs. Xu et al. [16] found that the addition of GNS improved the corrosion resistance of Sn-Ag-Cu solder. GNS is almost chemically inactive and serves as an inert physical barrier to prevent the formation and growth of corrosion products during the corrosion process. In addition, it was indicated that the corrosion resistance of solder is improved by the addition of Ni elements. Liu et al. [17] studied the corrosion behavior of Sn-9Zn-0.1X ($X = \text{Ni, Cr, Cu, and Ag}$) solder alloy. The

addition of the third element refined the intermetallic compound (IMC) and inhibited the formation of Zn-rich precipitate and the dissolution of the anodic solder. The corrosion resistance was significantly enhanced, since the addition of Ni to lead-free solder formed a dense passive film on the solder surface during the polarization test [18]. Huang et al. [19] found that the corrosion potential of Sn-9Zn- x Ni solder increased as the content of Ni increased. The electrochemical corrosion resistance is the best in 5 wt.% NaCl solution with the Ni content reaching 0.25 wt.%. Although the addition of carbon-based materials and nano-Ni particles can effectively improve the corrosion performance of lead-free solders, the disadvantages of nano-Ni particles is that they are prone to agglomerate, and carbon-based materials easily precipitate during melting, limiting their applications [20,21].

The metal organic framework (MOF), a porous material formed by self-assembly of organic ligands and metal ions through coordination bonds, is widely used in gas separation and storage, catalysis, and medicine transportation due to its large specific surface area and excellent adsorption properties [22,23]. The sheet-like Ni-MOF is synthesized by a traditional hydrothermal method, and a two-dimensional sheet-like structure with Ni nanoparticles embedded in the carbon skeleton is obtained after high-temperature carbonization. During the mixing of Ni@C and Sn-0.7Cu solder, the Ni nanoparticles are uniformly fixed by the carbon skeleton to avoid agglomeration of Ni nanoparticles. Furthermore, the Ni nanoparticles, which are fixed in the carbon skeleton, solve the problems of low activity and poor bonding of carbon materials during the melting process of solder due to their high activity.

In this paper, the electrochemical corrosion behavior of Sn-0.7Cu- x Ni@C composite solder in 3.5 wt.% NaCl solution was studied using a polarization curve. The microstructure and composition of the solder alloy after corrosion were characterized by scanning electron microscopy (SEM), X-ray diffraction (XRD), and X-ray photoelectron spectroscopy (XPS). The mechanism of Ni@C enhancement of the corrosion performance of Sn-0.7Cu lead-free solder was investigated.

2. Experimental

Ni-MOF was prepared by the conventional hydrothermal method. First, 0.84 g terephthalic acid (PTA), 0.264 g triethylenediamine (TED), and 1.44 g $\text{Ni}(\text{NO}_3)_2 \cdot 6\text{H}_2\text{O}$ were weighed, respectively, and dissolved into 120 mL of a mixture of N,N -dimethylformamide (DMF) and deionized water (DI) (2:1) with 30-min ultrasonic stirring. Subsequently, the mixture was placed in a hydrothermal reactor at 130 °C for 24 h, washed with DMF and ethanol three times, respectively, and dried under vacuum at 70 °C for 12 h. The obtained product was Ni-MOF. Ni@C was then generated after Ni-MOF was heated in a tube furnace at a ramping rate of 2 °C/min to 650 °C and maintained under Ar atmosphere for 6 h. Different mass fractions (0 wt.%, 0.04 wt.%, 0.08 wt.%, 0.12 wt.%) of Ni@C were weighed. The weighed Ni@C was placed in ethanol solution and ultrasonically dispersed for 15 min to obtain the Ni@C solution. The Ni@C solution, Sn powder, and Cu powder were placed in a ball mill tank and ground at 200 r/min for 6 h. Then the solder paste was dried to powder at 60 °C and pressed into blocks, each with a diameter of 16 mm. The solder blocks were heated to 500 °C for 30 min at a ramping rate of 8 °C/min under the atmosphere of Ar. The process was repeated four times.

As shown in Figure 1, a three-electrode system was employed to test the polarization curves in this study. The Sn-0.7Cu- x Ni@C solder was employed as the working electrode, the platinum electrode as the counter electrode, and the saturated glycerol electrode as the reference electrode. The composite solder was cut to a size of 10 × 10 × 3 mm to prepare the working electrode. Subsequently, the oxide film of the solder was removed by grinding with 800 mesh sandpaper, and the solder was tightly connected by conductive adhesive to the Cu wire. The specimens were placed in the mold with a 100 mm² surface reserved, solidified with epoxy resin for 2 h, and then polished with sandpaper (320–2000 mesh) and then subsequently polishing powder (0.05 μm). Polished samples were cleaned and dried with DI and alcohol. Before electrochemical testing, the samples were activated in 3.5 wt.%

NaCl solution for 30 min. The polarization curve parameters were set after stabilization of the open circuit potential whose potential scan range was -2.0 – 0.4 V with a scan speed of 10 mV/s. The whole process was conducted under normal temperature and pressure.

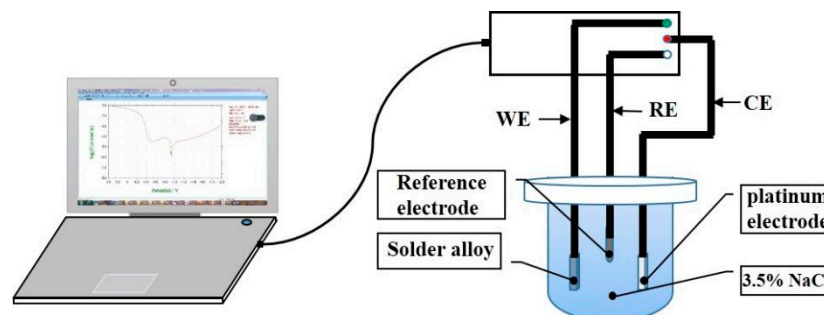


Figure 1. Schematic diagram of the classic three-electrode circuit.

Electrochemical experiments were performed via a CHI660D electrochemical workstation (Shanghai, China). The phases of corrosion products were analyzed by X-ray diffraction (XRD, D8-Advance, Bruker, Germany) with Cu K α radiation. The morphologies of specimens were characterized by scanning electron microscopy (SEM, Quanta 250, FEI, Hillsboro, OR, USA) and optical microscopy (OM, bx53, Olympus, Japan). The chemical compositions of specimens were analyzed by X-ray photoelectron spectroscopy (XPS, Escalab 250Xi, Thermo Scientific, Waltham, MA, USA).

3. Results and Discussion

3.1. Electrochemical Corrosion Properties of Sn-0.7Cu-*x*Ni@C Solder

The polarization curves of Sn-0.7Cu-*x*Ni@C composite solder are shown in Figure 2. It was noted that the potential scan rate had an important role in minimizing the effects of distortion in Tafel slopes and corrosion current density analyses, as previously reported [24–26]. However, based on these reports, the adopted 10 mV/s had no deleterious effects on the Tafel extrapolations in determining the corrosion current densities of the examined samples. The samples' corrosion current (i_{corr}) and corrosion voltage (E_{corr}) were obtained by the method of Tafel line extrapolation. The corrosion potential of Sn-0.7Cu was -1.008 V_{SCE}. After adding the strengthening phase Ni@C, the corrosion potential showed an upward trend. When the amount added was 0.04 wt.% and 0.08 wt.%, the corrosion potential was -0.981 V_{SCE} and -0.934 V_{SCE}, respectively. When the content of Ni@C increased to 0.12 wt.%, the corrosion potential dropped to -0.982 V_{SCE}. Furthermore, the corrosion current and corrosion potential of Sn-0.7Cu-*x*Ni@C were negatively correlated. The corrosion currents were 4.21×10^{-5} A/cm², 3.97×10^{-5} A/cm², 1.35×10^{-5} A/cm², and 1.64×10^{-5} A/cm² when the contents of Ni@C were 0% wt.%, 0.04 wt.%, 0.08 wt.%, and 0.12 wt.%, respectively. The results showed that Ni@C reduced the corrosion current of the composite solder, and the corrosion current dropped to the lowest level with the Ni@C amount added being 0.08 wt.%.

The electrochemical corrosion rate of metal is related to its corrosion current and corrosion potential. Specifically, high corrosion potential or low corrosion current can enhance metal corrosion resistance. As shown in Table S1, the corrosion potential and corrosion current were measured several times in this study. The variation pattern of corrosion potential and corrosion current showed that Ni@C enhanced the corrosion resistance of the composite solder with the best corrosion resistance of Sn-0.7Cu- 0.08 wt.% Ni@C solder. Furthermore, the corrosion rate of the composite solder could be calculated by Equation (1) [27], which confirmed this conclusion. As shown in Table 1, the corrosion rate of Sn-0.7Cu was 0.640 mm/y. As the content of Ni@C increased, the corrosion rate of the solder declined. It reduces to the lowest value of 0.205 mm/y, 67.9% less than that of Sn-0.7Cu when the content of Ni@C was 0.08 wt.%.

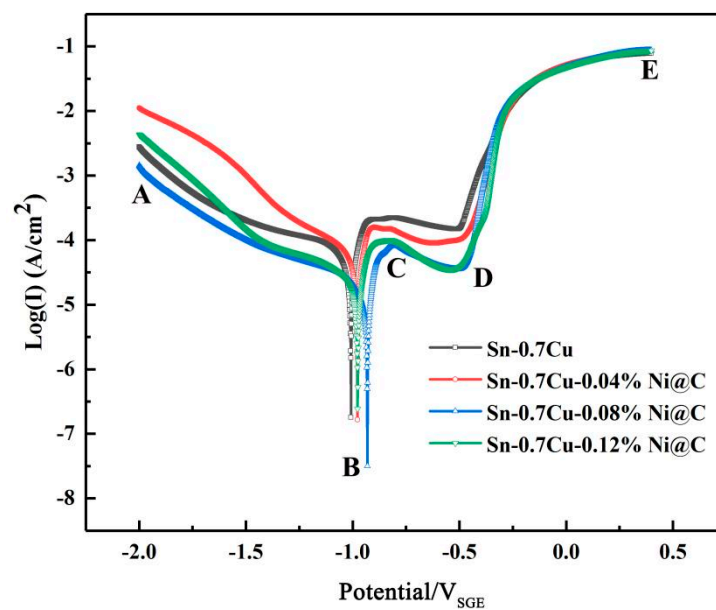


Figure 2. Polarization curve of Sn-0.7Cu-xNi@C ($x = 0, 0.04, 0.08, 0.12$ wt.%) composite solder in 3.5 wt.% NaCl solution.

$$R_{corr} = \frac{A \times i_{corr}}{n \times F \times \rho}, \quad (1)$$

where R_{corr} is the corrosion rate, A is the relative atomic mass of the solder, i_{corr} is the corrosion current density, n is the chemical valence of the element, F is a constant with a value of 26.8, and ρ is the density of the solder.

Table 1. Corrosion parameters of Sn-0.7Cu-xNi@C ($x = 0, 0.04, 0.08, 0.12$ wt.%) composite solder.

Composite Solder	E_{corr} (V _{SGE})	Error (%)	i_{corr} (A/cm ²)	Error (%)	Corrosion Rate (mm/y)
Sn-0.7Cu	−1.008	0.43	4.21×10^{-5}	1.11	0.640
Sn-0.7Cu-0.04 wt.% Ni@C	−0.981	0.41	3.97×10^{-5}	1.01	0.604
Sn-0.7Cu-0.08 wt.% Ni@C	−0.934	0.50	1.35×10^{-5}	1.48	0.205
Sn-0.7Cu-0.12 wt.% Ni@C	−0.982	0.34	1.64×10^{-5}	1.62	0.249

3.2. Analysis of Electrochemical Corrosion Process of Sn-0.7Cu-xNi@C Solder

The Sn-0.7Cu-xNi@C solder was characterized by XRD, as seen in Figure 3. The spectra of composite solders with different contents of Ni@C after electrochemical corrosion were the same, which indicated that Ni@C had no effect on the phases of corrosion products during electrochemical corrosion. Result showed that the phases of the composite solder after corrosion were $\text{Sn}_3\text{O}(\text{OH})_2\text{Cl}_2$, SnO, SnO_2 , Sn, and $(\text{Cu}, \text{Ni})_6\text{Sn}_5$ according to the XRD standard card (Figure S1). The corrosion products were mainly $\text{Sn}_3\text{O}(\text{OH})_2\text{Cl}_2$ because the peak intensities of SnO and SnO_2 were weak.

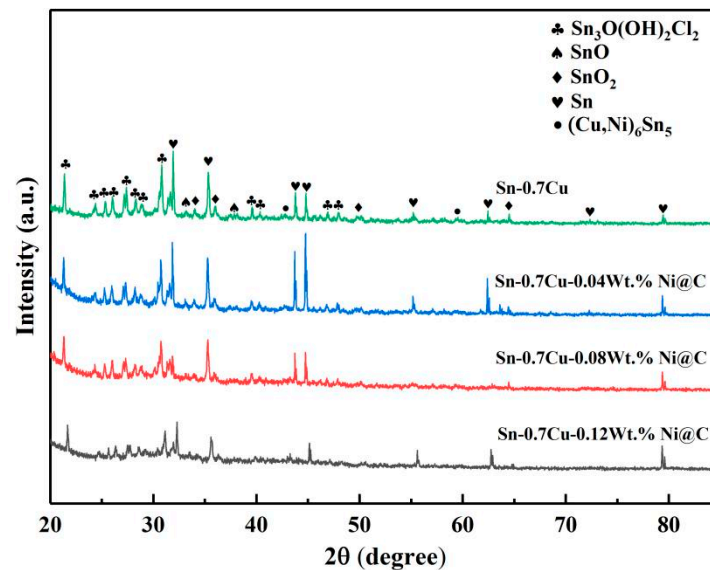


Figure 3. XRD pattern of Sn-0.7Cu- x Ni@C ($x = 0, 0.04, 0.08, 0.12$ wt.%) solder after electrochemical corrosion.

The surface of the corroded Sn-0.7Cu-0.08 wt.% Ni@C solder was examined by XPS to further verify the corrosion products of the composite solder, and the results are shown in Figure 4. The characteristic peaks of Sn, Cl, and O appear in the full spectrum of Figure 4a, indicating the involvement of these three elements in the chemical reaction. The characteristic peak of Sn $3d^{5/2}$ in the range of 490–484 eV was fitted for further analysis of the valence state. As shown in Figure 4b, Sn $3d^{5/2}$ consisted of three valence states, including Sn^{4+} , Sn^{2+} , and Sn^{0+} . The fitted result of O 1s in the range of 534–528 eV is shown in Figure 4c and indicates that the main valence states of O 1s were O^{2-} and OH^- , respectively. The OH^- was probably derived from the electrolytic water reaction at the cathode. The fitted result of Cl^- in the range of 204–196 eV is shown in Figure 4d. Cl^- with different binding strengths was speculated to be derived from NaCl and SnCl [28].

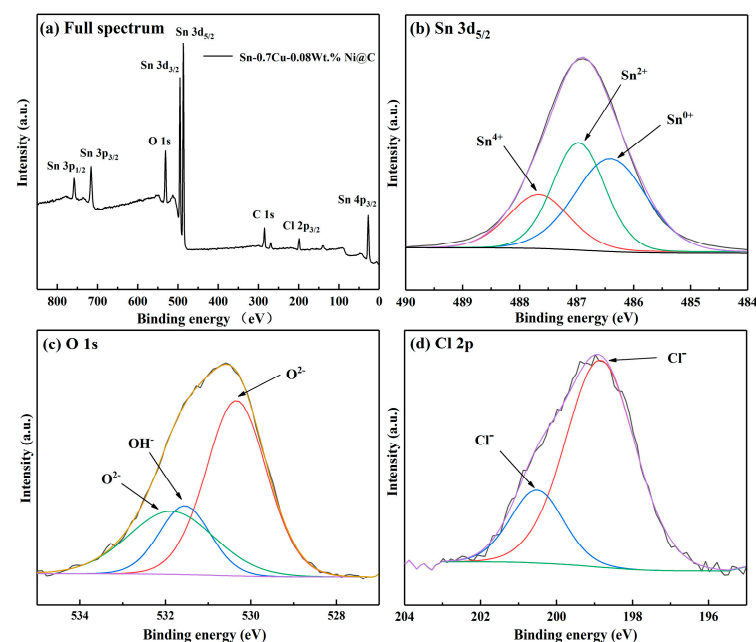
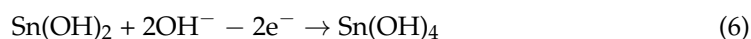
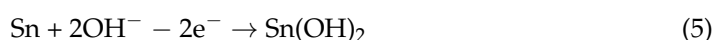


Figure 4. XPS images of Sn-0.7Cu-0.08 wt.% Ni@C after electrochemical corrosion: (a) full spectrum, (b) Sn $3d^{5/2}$, (c) O 1s, (d) Cl 2p.

The process of electrochemical corrosion is divided into anodic and cathodic reactions. As shown in Figure 2, similar trends in the polarization curves of all composite solders indicated that similar electrochemical reactions occurred on the surfaces of Sn-0.7Cu-*x*Ni@C solders during polarization reactions. The polarization reaction process of the composite solders was analyzed as an example of Sn-0.7Cu-0.08 wt.% Ni@C. The polarization curve is divided into four sections, including AB, BC, CD, and DE. The AB section is the process of the oxygen-consuming reduction reaction, which occurs at the cathode [29]. The reaction process is shown in Equation (2), in which the solder is not involved in the reaction process.



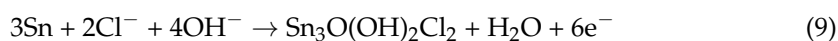
The BC, CD, and DE sections are the anodic reaction zones, where corrosion processes mainly occur. The point B is the turning point from the cathodic reaction to the anodic reaction, and the corresponding potential is the self-corrosion potential. The BC section is the dissolution stage, and the corrosion current density increases sharply with the increase of corrosion potential in this stage. Since the standard electrode potential of Sn is lower than that of the other metal elements (Cu and Ni) in the composite solder, the dissolution of Sn occurs mainly at this stage [30]. The reaction process is shown in Equations (3) and (4). During this process, the dissolution of Sn continues while other electrochemical reactions occur. As shown in Equations (5) and (6), a hydroxide of Sn is formed by the reaction of Sn with OH^- and free electrons [31].



$\text{Sn}(\text{OH})_2$ and $\text{Sn}(\text{OH})_4$ are hydrolyzed to be SnO and SnO_2 , respectively, as shown in Equations (7) and (8) [28].



In the CD stage, the hydroxide and oxide of Sn, generated on the surface of the composite solder, form a passivation film to protect the solder. The CD stage is thus known as the passivation stage. As shown in Figure 2, the current density decreased with the increase of Ni@C in the CD stage, and better protection was provided for the solder with the significantly increased passivation effect, which is closely related to its density. As shown in Figure 5, the β -Sn in the composite solder was gradually refined with increases in Ni@C. The refined β -Sn increased the density of the initial passive film and decreased the dissolution rate of the passive film [17]. The corrosion current increased sharply as the corrosion potential increased in the DE stage. It was concluded that a large amount of Cl^- was enriched on the surface layer of the passive film with the enhancement of the corrosion potential. When the amount reached a certain level, the passive film was broken down. The dissolution of Sn was accelerated by Cl^- , which led to the formation of the complexes of SnCl_3^- and SnCl_6^{2-} [32]. Thus, the corrosion current increased sharply. The final corrosion product $\text{Sn}_3\text{O}(\text{OH})_2\text{Cl}_2$ was generated by the reaction process of Equation (9) after the destruction of the passive film [33].



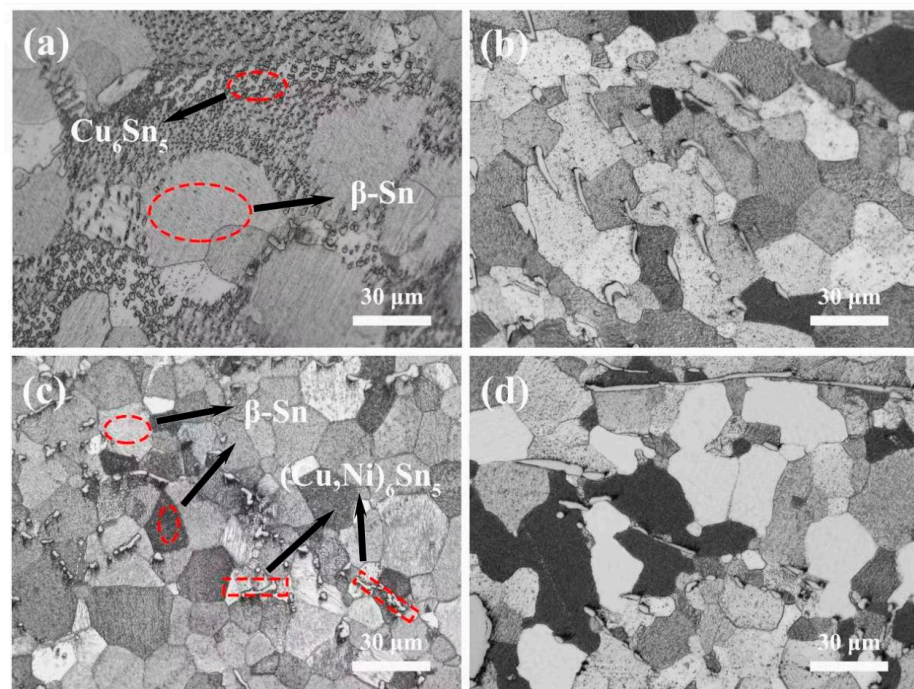


Figure 5. Metallographic microstructure diagram of Sn-0.7Cu- x Ni@C composite solder: (a) $x = 0$, (b) $x = 0.04$, (c) $x = 0.08$, (d) $x = 0.12$ wt.%.

Figure 5 shows the microstructures of the composite solder with the different contents of Ni@C. The microstructure of Sn-0.7Cu consisted of β -Sn grains and the reticulated Cu_6Sn_5 shown in Figure 5 [34]. With increasing Ni@C content, the IMC transformed from a reticulated structure to rod-like and dot-like, and the grains of β -Sn were gradually refined. When the added amount was 0.08 wt.%, the refinement effect achieved the best result. As shown in Figure 6, point A in Sn-0.7Cu-0.08 wt.% Ni@C solder was composed of the elements Sn, Cu, and Ni with the atomic ratio of 45.73:52.98:1.29. Therefore, IMC transformed from Cu_6Sn_5 to $(\text{Cu}, \text{Ni})_6\text{Sn}_5$ with the addition of Ni@C.

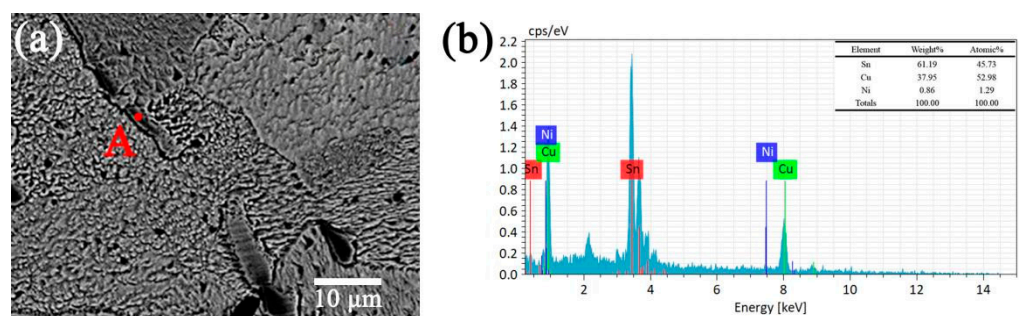


Figure 6. Microstructure (a) and EDS (b) of Sn-0.7Cu-0.08 wt.% Ni@C.

Figure 7 shows the final morphology of Sn-0.7Cu- x Ni@C solder after electrochemical corrosion. As shown in Figure 7a, the surface corrosion products of Sn-0.7Cu were thick flakes. The morphologies of corrosion products were refined into multi-layer flakes after the Ni@C was added. When the Ni@C content increased to 0.08 wt.%, corrosion products were further refined into a large quantity of fine needles and flakes, which made the corrosion products denser. When the content of Ni@C increased to 0.12 wt.%, the morphology was still needle-like and flake-like. However, as the proportion of flakes continued to increase, the corrosion products tended to coarsen. The dense corrosion products on the surface of the specimen could serve as physical barriers to prevent further erosion of Cl^- on the composite solder [35]. Figure 7a shows that the corrosion products of Sn-0.7Cu were locally

broken under the action of Cl^- , and that its surface was susceptible to Cl^- penetration. The corrosion products of Sn-0.7Cu-0.08 wt.% Ni@C solder were the densest, as shown in Figure 7c. The dense corrosion products increased the difficulty of Cl^- penetration and enhanced the corrosion resistance of the solder.

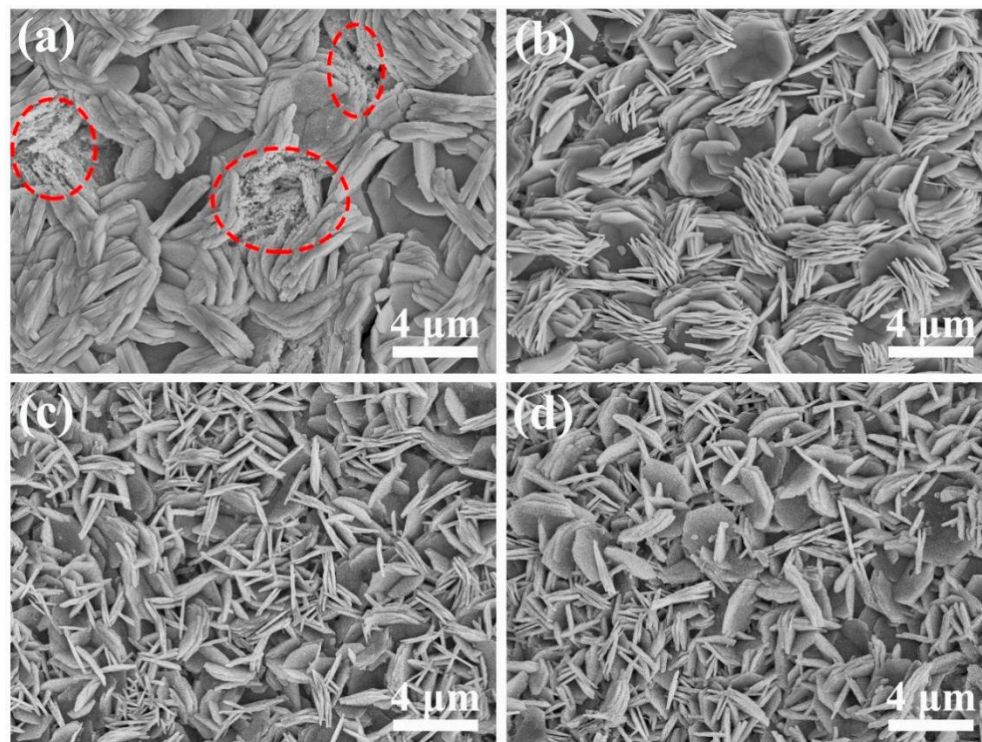


Figure 7. Surface morphology of Sn-0.7Cu- x Ni@C solder after electrochemical corrosion: (a) $x = 0$, (b) $x = 0.04$, (c) $x = 0.08$, (d) $x = 0.12$ wt.%.

3.3. Mechanism of Ni@C in Corrosion Process

The corrosion resistance of the composite solder with Ni@C was significantly enhanced. The Sn-0.7Cu- x Ni@C solder exhibited better corrosion resistance as the Ni@C content increased, which indicates that Ni@C plays a crucial role in improving corrosion resistance of the composite solder.

The corrosion behavior of the solder is closely related to its microstructure. The area ratio of cathode to anode has a significant impact on the corrosion resistance of the metal [36]. As shown in Figure 5, the grain refinement of β -Sn and $(\text{Cu}, \text{Ni})_6\text{Sn}_5$ was remarkable with the addition of Ni@C. The working area of the cathode remained unchanged while the Sn grains of the anode were refined, which brought about more corrosion micro-cells. Therefore, corrosion products increased in number and decreased in size. They extruded each other during the growth process to form a dense flake and needle-like corrosion layer. Consequently, the morphology of the corrosion products was gradually refined after the addition of Ni@C, and the rule of evolution was consistent with the refinement rule of the solder microstructure. The dense corrosion product $\text{Sn}_3\text{O}(\text{OH})_2\text{Cl}_2$ was attached to the surface of the solder. As the gaps between the corrosion products decreased, the refined corrosion products became more stable, which made it more difficult for Cl^- to break down corrosion products. As a result, the corrosion resistance of the composite solder was improved.

Furthermore, the carbon skeleton in Ni@C with poor chemical activity and excellent corrosion resistance was uniformly distributed in the composite solder, serving as a physical barrier to inhibit corrosion. Moreover, the carbon skeleton distributed in the solder increased the curvature of the diffusion path of oxygen atoms, which enhanced the oxygen

barrier properties of the solder [16]. Therefore, the dissolution process of the anode solder was alleviated, and corrosion resistance of composite solder was improved.

Furthermore, the IMC played a critical role in the corrosion process of solder [37]. On the one hand, the Cu-Sn compound transformed from Cu_6Sn_5 to $(\text{Cu}, \text{Ni})_6\text{Sn}_5$ with the addition of Ni@C. Due to the synergistic effect of Ni and carbon skeleton, the grains of IMC were obviously refined, which resulted in a reduction in the cathode surface area. Thus, the area ratio of the cathode to the anode became smaller, which reduced the corrosion rate of the galvanic couple and inhibited the dissolution of Sn in the anode. On the other hand, since the electrode potential of Cu (+0.5210 V) was greater than that of Sn, an obvious potential difference existed between β -Sn and Cu_6Sn_5 in the Sn-0.7Cu solder. The standard electrode potential of Ni is -0.2570 V, so the electrode potential of $(\text{Cu}, \text{Ni})_6\text{Sn}_5$ was lower than that of Cu_6Sn_5 , but higher than that of Sn.

After Ni@C was added, the potential difference between IMC and β -Sn in the solder gradually decreased, which reduced the galvanic corrosion rate. As a result, the corrosion resistance of the composite solder was boosted. However, when the addition amount of Ni@C exceeded 0.08 wt.%, Ni@C agglomerated gradually, resulting in the coarsening of β -Sn and IMC. Thus, the effect of Ni@C on the enhancement of corrosion resistance of composite solder was reduced.

4. Conclusions

In this paper, Ni@C was added to Sn-0.7Cu solder to improve its corrosion resistance. The results show that the corrosion rate of the composite solder decreased with the addition of Ni@C and reduced to a minimum value of 0.205 mm/y when the content of Ni@C reached 0.08 wt.%. The corrosion product of the composite solder was mainly $\text{Sn}_3\text{O}(\text{OH})_2\text{Cl}_2$. Moreover, resulting from the refinement of β -Sn and IMC, the morphologies of corrosion products were transformed from thick flakes to fine needles and thin flakes and became dense with increasing Ni@C content. The dense corrosion products increased the difficulty of Cl^- penetration and enhanced the corrosion resistance of the solder. The carbon skeleton in Ni@C, serving as a physical barrier with low activity, inhibited corrosion. Furthermore, with the addition of Ni@C, the potential difference between IMC and β -Sn decreased, which reduced the corrosion rate of the galvanic couple.

Supplementary Materials: The following are available online at <https://www.mdpi.com/article/10.3390/met12071172/s1>, Table S1: Corrosion parameters of Sn-0.7Cu-xNi@C ($x = 0, 0.04, 0.08, 0.12$ Wt.%) composite solder; Figure S1: XRD pattern of Sn-0.7Cu-xNi@C ($x = 0, 0.04, 0.08, 0.12$ Wt.%) solder after electrochemical corrosion.

Author Contributions: Conceptualization, G.L. and B.L.; methodology, G.L. and B.L.; validation, Z.G. and Y.L.; formal analysis, Z.G. and Y.L.; investigation, G.L.; resources, Y.L. and F.W.; data curation, B.L. and G.L.; writing—original draft preparation, F.W.; writing—review and editing, F.W. and G.L.; supervision, B.L.; project administration, G.L. All authors have read and agreed to the published version of the manuscript.

Funding: This work was supported by the “Fundamental Research Funds for the Central Universities” (2020ZDPYMS37) and “Frontier Leading Technology Basic Research Project (Xuzhou, China)” (KC21009).

Institutional Review Board Statement: Not applicable.

Informed Consent Statement: Not applicable.

Data Availability Statement: Not applicable.

Conflicts of Interest: The authors declare no conflict of interest.

References

1. Ma, H.; Suhling, J.C. A review of mechanical properties of lead-free solders for electronic packaging. *J. Mater. Sci.* **2009**, *44*, 1141–1158. [[CrossRef](#)]

2. Griffiths, S.; Wedi, A.; Schmitz, G. Work of adhesion and reactive wetting in SnPb/Cu,Ni and SnBi/Cu,Ni soldering systems. *Mater. Charact.* **2021**, *178*, 111304. [\[CrossRef\]](#)
3. Siahaan, E. Behavior of Sn-0.7Cu-xZn lead free solder on physical properties and micro structure. *IOP Conf. Ser. Mater. Sci. Eng.* **2017**, *237*, 012044. [\[CrossRef\]](#)
4. Zhao, M.; Zhang, L.; Liu, Z.Q.; Xiong, M.Y.; Sun, L. Structure and properties of Sn-Cu lead-free solders in electronics packaging. *Sci. Technol. Adv. Mater.* **2019**, *20*, 421–444. [\[CrossRef\]](#)
5. Zhang, Q.; Hu, F.; Song, Z. Transient Soldering Reaction Mechanisms of SnCu Solder on CuNi Nano Conducting Layer and Fracture Behavior of the Joint Interfaces. *J. Electron. Mater.* **2020**, *49*, 3383–3390. [\[CrossRef\]](#)
6. Zhou, H.; Guo, J.; Shang, J.; Song, X. Highly solderability of FeP film in contact with SnAgCu solder. *J. Alloys Compd.* **2020**, *818*, 152900. [\[CrossRef\]](#)
7. Tian, R.; Hang, C.; Tian, Y.; Zhao, L. Growth behavior of intermetallic compounds and early formation of cracks in Sn-3Ag-0.5Cu solder joints under extreme temperature thermal shock. *Mater. Sci. Eng. A* **2018**, *709*, 125–133. [\[CrossRef\]](#)
8. Guo, W.; Ma, X.; Gao, M.; Yan, J. Direct soldering of screen-printed Al-paste layer on back-side of silicon solar cell using SnAg solder. *Mater. Lett.* **2018**, *231*, 146–149. [\[CrossRef\]](#)
9. Zhang, P.; Xue, S.; Wang, J. New challenges of miniaturization of electronic devices: Electromigration and thermomigration in lead-free solder joints. *Mater. Des.* **2020**, *192*, 108726. [\[CrossRef\]](#)
10. Qu, D.; Li, C.; Bao, L.; Kong, Z.; Duan, Y. Structural, electronic, and elastic properties of orthorhombic, hexagonal, and cubic Cu₃Sn intermetallic compounds in Sn–Cu lead-free solder. *J. Phys. Chem. Solids* **2020**, *138*, 109253. [\[CrossRef\]](#)
11. Osório, W.R.; Spinelli, J.E.; Afonso, C.R.M.; Peixoto, L.C.; Garcia, A. Microstructure, corrosion behaviour and microhardness of a directionally solidified Sn–Cu solder alloy. *Electrochim. Acta* **2011**, *56*, 8891–8899. [\[CrossRef\]](#)
12. Lv, Y.; Yang, W.; Mao, J.; Li, Y.; Zhang, X.; Zhan, Y. Effect of graphene nano-sheets additions on the density, hardness, conductivity, and corrosion behavior of Sn–0.7Cu solder alloy. *J. Mater. Sci. Mater. Electron.* **2019**, *31*, 202–211. [\[CrossRef\]](#)
13. Subri, N.W.B.; Sarraf, M.; Nasiri-Tabrizi, B.; Ali, B.; Mohd Sabri, M.F.; Basirun, W.J.; Sukiman, N.L. Corrosion insight of iron and bismuth added Sn–1Ag–0.5Cu lead-free solder alloy. *Corros. Eng. Sci. Technol.* **2019**, *55*, 35–47. [\[CrossRef\]](#)
14. Rosalbino, F.; Angelini, E.; Zanichchi, G.; Marazza, R. Corrosion behaviour assessment of lead-free Sn–Ag–M (M=In, Bi, Cu) solder alloys. *Mater. Chem. Phys.* **2008**, *109*, 386–391. [\[CrossRef\]](#)
15. Han, Y.D.; Chen, L.; Jing, H.Y.; Nai, S.M.L.; Wei, J.; Xu, L.Y. Effect of Ni-Coated Carbon Nanotubes on the Corrosion Behavior of Sn–Ag–Cu Solder. *J. Electron. Mater.* **2013**, *42*, 3559–3566. [\[CrossRef\]](#)
16. Xu, L.Y.; Zhang, Z.K.; Jing, H.Y.; Wei, J.; Han, Y.D. Effect of graphene nanosheets on the corrosion behavior of Sn–Ag–Cu solders. *J. Mater. Sci. Mater. Electron.* **2015**, *26*, 5625–5634. [\[CrossRef\]](#)
17. Liu, J.-C.; Wang, Z.-H.; Xie, J.-Y.; Ma, J.-S.; Shi, Q.-Y.; Zhang, G.; Suganuma, K. Effects of intermetallic-forming element additions on microstructure and corrosion behavior of Sn–Zn solder alloys. *Corros. Sci.* **2016**, *112*, 150–159. [\[CrossRef\]](#)
18. Mohanty, U.S.; Lin, K.-L. Corrosion Behavior of Pb-Free Sn-1Ag-0.5Cu-XNi Solder Alloys in 3.5% NaCl Solution. *J. Electron. Mater.* **2013**, *42*, 628–638. [\[CrossRef\]](#)
19. Huang, M.L.; Kang, N.; Zhou, Q.; Huang, Y.Z. Effect of Ni Content on Mechanical Properties and Corrosion Behavior of Al/Sn–9Zn–xNi/Cu Joints. *J. Mater. Sci. Technol.* **2012**, *28*, 844–852. [\[CrossRef\]](#)
20. Han, Y.; Li, W.; Zhang, M.; Tao, K. Catalytic dechlorination of monochlorobenzene with a new type of nanoscale Ni(B)/Fe(B) bimetallic catalytic reductant. *Chemosphere* **2008**, *72*, 53–58. [\[CrossRef\]](#)
21. Yang, Z.; Zhou, W.; Wu, P. Effects of Ni-coated carbon nanotubes addition on the microstructure and mechanical properties of Sn–Ag–Cu solder alloys. *Mater. Sci. Eng. A* **2014**, *590*, 295–300. [\[CrossRef\]](#)
22. Zhu, D.; Liu, J.; Wang, L.; Du, Y.; Zheng, Y.; Davey, K.; Qiao, S.Z. A 2D metal-organic framework/Ni(OH)₂ heterostructure for an enhanced oxygen evolution reaction. *Nanoscale* **2019**, *11*, 3599–3605. [\[CrossRef\]](#) [\[PubMed\]](#)
23. Leea, C.S.; Limb, J.M.; Parkb, J.T.; Kima, J.H. Direct growth of highly organized, 2D ultra-thin nano-accordion Ni-MOF@NiS₂@C core-shell for high performance energy storage device. *Chem. Eng. J.* **2021**, *406*, 126810. [\[CrossRef\]](#)
24. Duarte, T.; Meyer, Y.A.; Osório, W.R. The Holes of Zn Phosphate and Hot Dip Galvanizing on Electrochemical Behaviors of Multicoatings on Steel Substrates. *Metals* **2022**, *12*, 863. [\[CrossRef\]](#)
25. Zhang, X.L.; Jiang, Z.H.; Yao, Z.P.; Song, Y.; Wu, Z.D. Effects of scan rate on the potentiodynamic polarization curve obtained to determine the Tafel slopes and corrosion current density. *Corros. Sci.* **2009**, *51*, 581–587. [\[CrossRef\]](#)
26. McCafferty, E. Validation of corrosion rates measured by Tafel extrapolation method. *Corros. Sci.* **2005**, *47*, 3202–3215. [\[CrossRef\]](#)
27. Yingsamphancharoen, T.; Srisuwan, N.; Rodchanarowan, A. The Electrochemical Investigation of the Corrosion Rates of Welded Pipe ASTM A106 Grade B. *Metals* **2016**, *6*, 207. [\[CrossRef\]](#)
28. Wang, M.; Wang, J.; Feng, H.; Ke, W. Effect of Ag₃Sn intermetallic compounds on corrosion of Sn-3.0Ag-0.5Cu solder under high-temperature and high-humidity condition. *Corros. Sci.* **2012**, *63*, 20–28. [\[CrossRef\]](#)
29. Fayeka, M.; Fazal, M.A.; Haseeb, A.S.M.A. Effect of aluminum addition on the electrochemical corrosion behavior of Sn–3Ag–0.5Cu solder alloy in 3.5 Wt.% NaCl solution. *J. Mater. Sci. Mater. Electron.* **2016**, *27*, 12193–12200. [\[CrossRef\]](#)
30. Lao, X.-D.; Cheng, C.-Q.; Min, X.-H.; Zhao, J.; Zhou, D.-Y.; Wang, L.-H.; Li, X.-G. Corrosion and leaching behaviors of Sn-based alloy in simulated soil solutions. *Trans. Nonferr. Met. Soc. China* **2016**, *26*, 581–588. [\[CrossRef\]](#)
31. Li, D.; Conway, P.P.; Liu, C. Corrosion characterization of tin-lead and lead free solders in 3.5 wt.% NaCl solution. *Corros. Sci.* **2008**, *50*, 995–1004. [\[CrossRef\]](#)

32. Jaffery, H.A.; Mohd Sabri, M.F.; Rozali, S.; Mahdavi, M.H.; Shnawah, D.A. Effect of temperature and alloying elements (Fe and Bi) on the electrical resistivity of Sn-0.7Cu solder alloy. *RSC Adv.* **2016**, *6*, 58010–58019. [[CrossRef](#)]
33. Jaffery, H.A.; Sabri, M.F.M.; Said, S.M.; Hasan, S.W.; Sajid, I.H.; Nordin, N.I.M.; Megat Hasnan, M.M.I.; Shnawah, D.A.; Moorthy, C.V. Electrochemical corrosion behavior of Sn-0.7Cu solder alloy with the addition of bismuth and iron. *J. Alloys Compd.* **2019**, *810*, 151925. [[CrossRef](#)]
34. Yu, C.Y.; Lee, T.K.; Tsai, M.; Liu, K.C.; Duh, J.G. Effects of Minor Ni Doping on Microstructural Variations and Interfacial Reactions in Cu/Sn-3.0Ag-0.5Cu-xNi/Au/Ni Sandwich Structures. *J. Electron. Mater.* **2010**, *39*, 2544–2552. [[CrossRef](#)]
35. Li, Q.; Zhao, M.; Lin, J.; Lu, S. Effect of temperature on the corrosion behavior of lead-free solders under polyvinyl chloride fire smoke atmosphere. *J. Mater. Res. Technol.* **2021**, *15*, 3088–3098. [[CrossRef](#)]
36. Osório, W.R.; Garcia, L.R.; Peixoto, L.C.; Garcia, A. Electrochemical behavior of a lead-free SnAg solder alloy affected by the microstructure array. *Mater. Des.* **2011**, *32*, 4763–4772. [[CrossRef](#)]
37. Gharaibeh, A.; Felhósi, I.; Keresztes, Z.; Harsányi, G.; Illés, B.; Medgyes, B. Electrochemical Corrosion of SAC Alloys: A Review. *Metals* **2020**, *10*, 1276. [[CrossRef](#)]